Wang *et al.*
Terrestrial, Atmospheric and Oceanic Sciences (2025) 36:17
https://doi.org/10.1007/s44195-025-00102-z

Terrestrial, Atmospheric and Oceanic Sciences

RESEARCH Open Access

Fast report: near-real-time assessment of the M_L6.4 Dapu earthquake-induced landslides

Kai-Shyr Wang[1], Wei-An Chao[2,3*], Che-Ming Yang[4], Tz-Shin Lai[1,5] and Yih-Min Wu[1,6]

Abstract

Rapid assessment of potential landslides in regions of risk and their associated impacts following an earthquake is needed to provide crucial information to guide emergency responses. After the 2025 M6.4 Dapu earthquake in southern Taiwan, we applied a combined analysis of Newmark displacement and a decision tree model to rapidly identify slopes with a high potential for failure. Then, the coseismic landslide inventory taken in the weeks following the Dapu earthquake was compiled from satellite images in conjunction with field photographs. In total, 45 landslides were identified. According to the available near-real-time earthquake shaking proxies and landslide inventories, most landslides occurred within the 250 gal, 15 cm/s and 0.3 cm contour lines of earthquake shaking associated with peak ground acceleration (PGA), peak ground velocity (PGV) and peak vertical displacement of 3-s P waves (Pd3), respectively. In addition, we found that a peak vertical displacement (Pd) larger than 0.3 cm is a good indicator for identifying coseismic landslides and can provide sufficient lead times (LTs) of 3–5 s for emergency response. Our work can serve as a basis for advancing conventional susceptibility assessment after an earthquake occurrence to achieve a coseismic landslide early warning (CoLEW) system.

Keywords Coseismic landslide, Lead time, Coseismic landslide early warning

1 Introduction

Coseismic landslides, which are one of the most common geologic hazards triggered by earthquakes, can cause extensive damage and result in significant economic losses and casualties (Keefer, 1994). To better understand the patterns of occurrence and factors influencing coseismic landslides, the method for predicting landslide susceptibility, which provides the probability of landslide occurrence in a given area and is helpful for rapidly assessing landslide hazards, has been widely developed in recent decades (Guzzetti et al. 1999; Lee 2014; Nowicki Jessee et al. 2018; Pham et al. 2018; Chung et al. 2021; Lai et al. 2024). These studies have comprehensively analyzed the relationships between coseismic landslides and lithology, topographic features, earthquake shaking, earthquake source mechanisms and tectonics. To characterize shaking associated with earthquake-triggered landslides, numerous studies have used simple proxies, such as peak ground acceleration (PGA), peak ground velocity (PGV) and Arias intensity, which are often extracted from real-time strong-motion records and can be used to quickly evaluate the specific locations of coseismic landslides (Harp and Wilson 1995; Harp et al. 2014; Chousianitis

*Correspondence:
Wei-An Chao
vvnchao@gmail.com; vvnchao@nycu.edu.tw
[1] Department of Geosciences, National Taiwan University, Taipei 10617, Taiwan
[2] Department of Civil Engineering, National Yang Ming Chiao Tung University, Hsinchu 30010, Taiwan
[3] Disaster Prevention and Water Environment Research Center, National Yang Ming Chiao Tung University, Hsinchu 30010, Taiwan
[4] Department of Civil and Disaster Prevention Engineering, National United University, Miaoli 36063, Taiwan
[5] Seismological Observation Center, Central Weather Administration, Taipei 100006, Taiwan
[6] Institute of Earth Sciences, Academia Sinica, Taipei 11529, Taiwan

© The Author(s) 2025. **Open Access** This article is licensed under a Creative Commons Attribution 4.0 International License, which permits use, sharing, adaptation, distribution and reproduction in any medium or format, as long as you give appropriate credit to the original author(s) and the source, provide a link to the Creative Commons licence, and indicate if changes were made. The images or other third party material in this article are included in the article's Creative Commons licence, unless indicated otherwise in a credit line to the material. If material is not included in the article's Creative Commons licence and your intended use is not permitted by statutory regulation or exceeds the permitted use, you will need to obtain permission directly from the copyright holder. To view a copy of this licence, visit http://creativecommons.org/licenses/by/4.0/.

et al. 2016; Chang et al. 2024; Lai et al. 2024) for rapid assessment and hazard mitigation. For example, most coseismic landslides induced by the 2024 Hualien earthquake have had PGA values > 250 gal (1 gal = 1 cm/s^2) and PGV values > 15 cm/s (Chang et al. 2024). However, Rault et al. (2020) reported a complex seismic response due to subsurface geology and topographic effects and demonstrated that the frequency and amplitude of seismic ground motion due to topographic amplification are controlled mainly by the shape, size, and elongation of a ridge. Therefore, detailed investigation and evaluation of each site is essential in landslide susceptibility assessment. With the available prediction model of earthquake ground shaking, a synthetic shaking scenario from hypothesized information of earthquake magnitude and location can be easily calculated and applied into the landslide susceptibility model, resulting in a coseismic landslide probability map. The aforementioned information provides the potential exposure to future coseismic landslide before earthquake occurrence (Lee 2014; Pham et al. 2018). In a postseismic case, combining near-real-time recording of earthquake ground shaking with the susceptibility model can rapidly assess the distribution of coseismic landslides within minutes of earthquake occurrence (Nowicki Jessee et al. 2018; Chuang et al. 2021).

Over the past decade, the peak ground displacement amplitude of the initial P-wave motion (Pd) was proposed for threshold-based earthquake early warning (EEW), which has been used as an indicator of structural damage to buildings (Shieh et al. 2011), emergency stops along high-speed railways (Wu et al. 2011), and potential damage zones (Hsieh et al. 2015; Wu et al. 2016). Pd amplitudes ranging from 0.2 to 0.5 cm have been proposed to be good indicators of earthquake destructiveness (Wu and Kanamori 2005; Shieh et al. 2011; Colombelli et al. 2012). In the threshold-based method, once the Pd value exceeds a specific threshold, an alarm is issued. Thus, a certain Pd threshold can probably be used to identify potential landslide zones during an earthquake. Compared with the landslide susceptibility model, the Pd-based approach provides the lead time (LT) before peak ground shaking (e.g., PGA, PGV) arrives. A few seconds of LT is sufficient for decision-making regarding emergency evacuation. People using roads can move into highway tunnels and/or to the evacuation route. To date, however, the aforementioned potential of the coseismic landslide early warning (CoLEW) system has not yet been explored.

At 16:17 on January 20, 2025 (UTC), the M_L 6.4 Dapu earthquake struck southwestern Taiwan (Wu et al. 2025), specifically Tainan and Chiayi. The Dapu earthquake was a reverse-slip earthquake (IES-RMT, https://rmt.earth.sinica.edu.tw) with a focal depth of 9.7 km at 120.57°E and 23.23°N, as reported by the Central Weather Administration (CWA). Our study first inspected the area with earthquake shaking larger than or equal to PGA = 250 gal, corresponding to an upper limit of CWA seismic intensity 5+, to map coseismic landslides using satellite images. A total of 45 landslides were detected. By combining the coseismic landslide inventory with estimates of ground shaking, we present the first results of the empirical relationships between Pd and the distribution of coseismic landslides. A certain Pd-based threshold enables the calculation of the early warning LT for an emergency response. Our results demonstrate the potential for the Pd proxy to provide new insights into the CoLEW and highlight needs that are relevant to a comprehensive examination of the Pd threshold for providing sufficient LT.

2 Strong-motion records and shaking proxies

We collected near-real-time strong-motion records of the Dapu earthquake from the GDMS-2020 website (https://gdms.cwa.gov.tw/, last accessed February 2025). In total, 425 strong-motion records were processed. The preprocessing of the raw three-component (north, east, and vertical) acceleration data included removing both the mean and linear trends. Then, we calculated the vector sum of the three-component accelerations, which is the sum of squaring the strong ground motion followed by taking the square root. Finally, the PGA was found by identifying the maximum value from the acceleration time series. The time series of ground velocity and displacement was obtained from acceleration records once and a double-integration time, respectively. High-pass filtering with a 0.075 Hz corner frequency was applied to the time series after the integration process, which can remove the long-period drift caused by the strong shaking (Shieh et al. 2011). PGV was directly estimated from the vector sum of the three-component velocities. In this study, Pd3 was measured from the filtered vertical displacement record over a 3-s time window after the arrival of the P-wave (t_p). t_p was automatically detected from acceleration records by a deep-neural-network-based picking method (PhaseNet) developed by Zhu and Beroza (2019). The LT was defined as the time interval between the time of the exceedance of the filtered vertical displacement of 0.3 cm (t_{Pd}) and that of the PGA (t_{PGA}). For a given station, there is no LT if t_{Pd} occurs later than t_{PGA}. Shake map and early warning LT distribution from CWA real-time strong motion network are shown in Fig. 1a, b. Figure 1c, d display examples of the summarized vectors of three-component acceleration and velocity records and the corresponding filtered vertical displacement waveforms. The time points associated with the earthquake shaking proxies, such as the PGA, PGV, Pd3, and Pd, can be found in

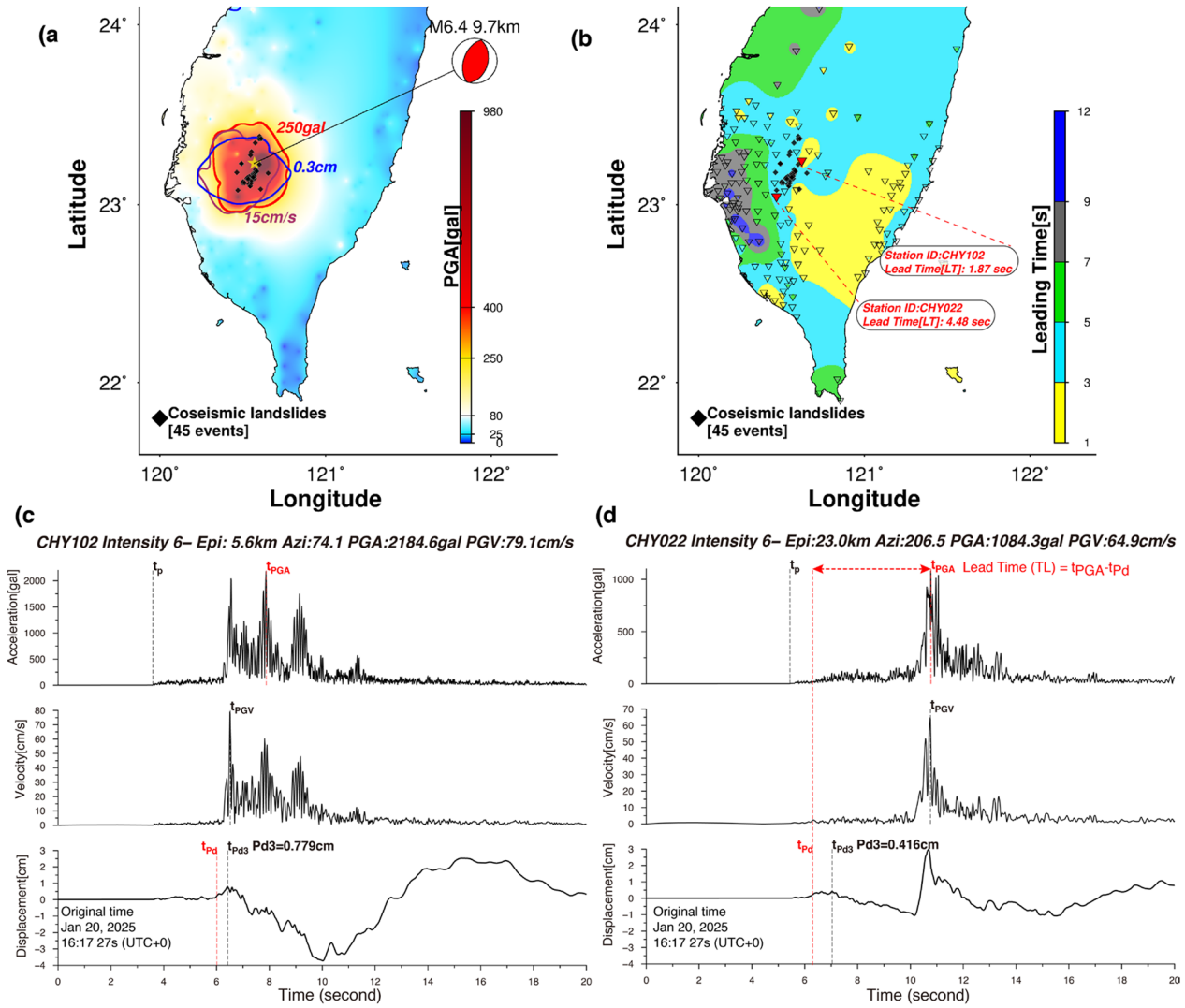

Fig. 1 Distributions of the (**a**) PGA and (**b**) lead time (LT) readings. The contours on the plots show the isolines related to the shaking proxies of PGA = 250 gal (red), PGV = 15 cm/s (pink) and Pd3 = 0.3 cm (blue). The solid diamonds indicate the coseismic landslides triggered by the Dapu earthquake. Examples showing the time points of Pd, Pd3, PGA, PGV and P-wave arrival measurements marked by vertical dashed lines for stations (**c**) CHY102 and (**d**) CHY022. Pd3 is the peak displacement amplitude within the 3-s window after the P-wave arrival time (t_p). LT is determined by the time interval of the two red dashed lines corresponding to the time points of displacement (Pd) larger than 0.3 cm and the PGA

Fig. 1c, d. All waveforms used in this study were manually checked to avoid artificial error involved in our data analysis.

3 Mapping and susceptibility assessment of coseismic landslides

The webpage of the CoSeismic landslide Susceptibility (CSS, https://css.lab.nycu.edu.tw; Lai et al. 2024) map has been operated since 2024 for 175 potential planar failure slopes as target slopes (TSs) with lithologies of sandstone and/or sandstone interbedded with shale and slope areas larger than 10 hectares. After the Dapu earthquake, the CSS system reported traffic light-based signals (green: normal; yellow: low risk; orange: medium risk; and red: high risk) of potential TSs, which indicate the levels of risk for coseismic landslides. Only stations with PGA > 196 gal and d10 (the cumulative Newmark displacement within 10 s) > 10 cm were selected to be the pair of representative stations (RS) and TS. For each RS-TS pair, the five input variables of PGA, PGV, epicentral distance and azimuth for RS, and strike of TS were used in the model prediction. On the basis of the C5.0 decision tree model trained on data for all of Taiwan, the prediction results of the model revealed that

among the 54 TSs identified by 16 RSs, 31 TSs were classified as normal (green), 1 TS was classified as low risk (yellow), 2 TSs were classified as medium risk (orange), and 20 TSs were classified as high risk (red) (colored dots in Fig. 2a). A more detailed methodology associated with the procedure involved in the CSS system is provided by Lai et al. (2024).

In this study, satellite imagery was employed to identify and delineate coseismic landslides. The pre-earthquake imagery was obtained from Sentinel-2 on December 20,

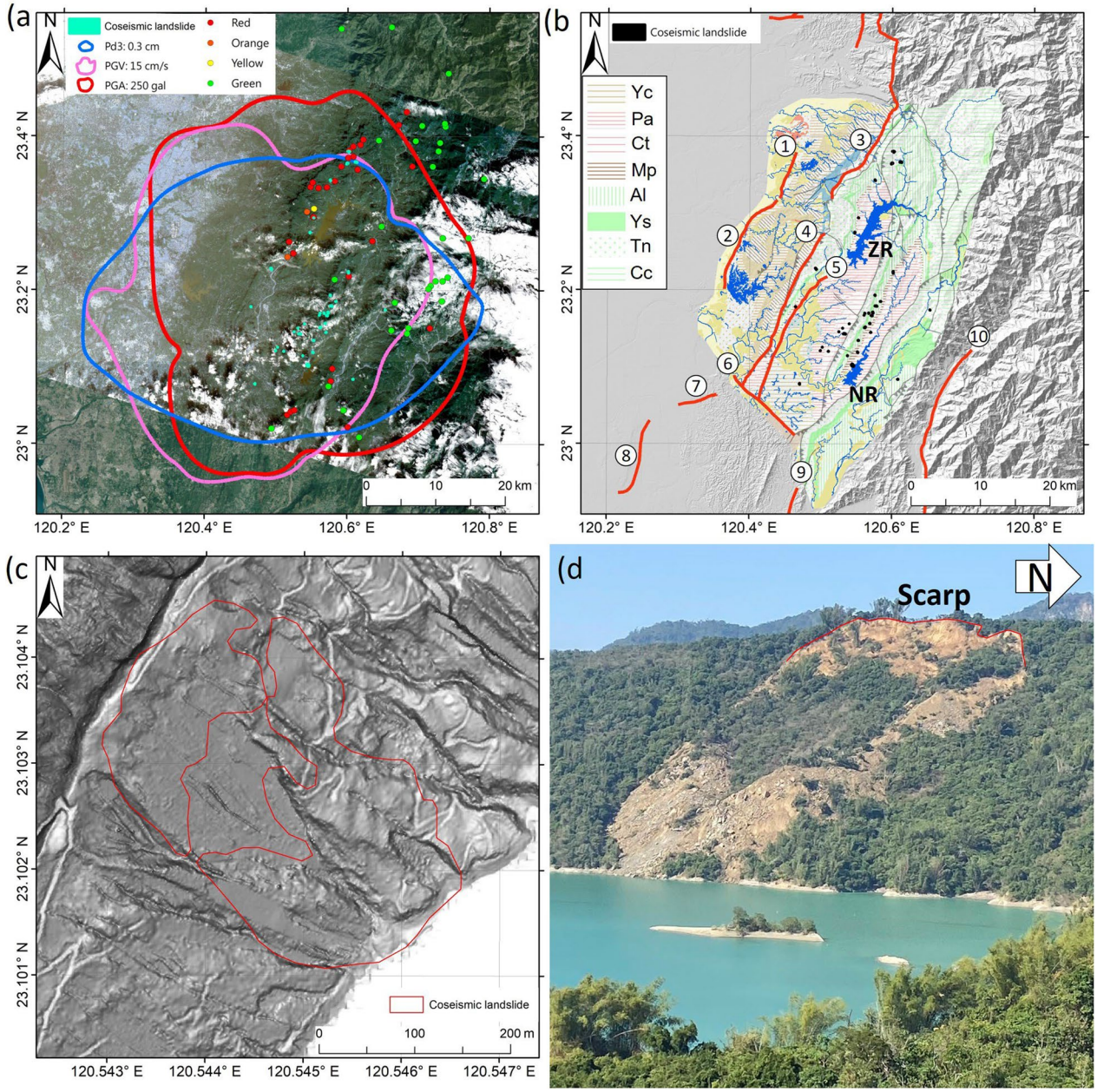

Fig. 2 (**a**) Distribution of the coseismic landslide inventory with contours of PGA, PGV and Pd3 and traffic light-based CSS depicted by colored dots (green: normal; yellow: low risk; orange: medium risk; red: high risk). The background is the post-earthquake SPOT6 image; (**b**) geologic map of the study area, with active faults represented by red lines (Fault: 1. Mujiliao fault, 2. Liujia fault, 3. Chukou Fault, 4. Lunhou Fault, 5. Kouhsiaoli Fault, 6. Tsochen Fault; 7. Hsinhua Fault; 8. Houchiali Fault, 9. Chekualin Fault, 10. Chaochou Fault). ZR: Zenwen Reservoir, NR: Nanhua Reservoir. The legend shows only the Formations of coseismic landslides (refer to the footnote of Table 1) (Fei and Chen 2013; Lin et al. 2007, 2009, 2021). (**c**) One meter-high-resolution LiDAR slope map and (**d**) photograph of the largest coseismic landslide (event Nos. 6 and 7 in Table 1). The scarp is clear, but the thickness of the sliding mass is difficult to evaluate via photography

2024, whereas the post-earthquake images were captured by SPOT 6 on January 22, 2025, and by Sentinel-2 on January 24, 2025. The image resolutions of Sentinel-2 and SPOT 6 are 10 m and 1.5 m, respectively. A total of 45 landslides were identified by manually (area marked in cyan in Fig. 2a), with the majority of landslides situated in regions where the PGA exceeds 250 gal, the PGV surpasses 15 cm/s, and Pd3 is greater than 0.3 cm (red, pink and blue lines shown in Fig. 1a). The average slope and aspect of the identified coseismic landslides are approximately 36.6° and 136°, respectively. The elevations of the landslides range from 92 to 1,120 m, with a mean elevation of 530 m. The geological formations associated with these landslides are illustrated in Fig. 2b and detailed in Table 1. The cumulative area of the coseismic landslide inventory is 258, 113 m^2, with individual landslide areas varying from 506 to 47,492 m^2. Notably, the largest coseismic landslide, which is located near the Nanhua Reservoir dam, consists of two polygons on a dip slope; when these polygons are combined, the total area is 70,202 m^2 (event Nos. 6 and 7 in Table 1; Fig. 2c). Field photographs and topographic features suggest the potential for planar sliding (illustrated in Fig. 2d). This potential failure zone is situated within the reservoir area, and if a catastrophic landslide occurs, it could possibly lead to surges or oscillations in water levels, potentially triggering flooding or further slope failure. Consequently, a comprehensive geological investigation is imperative to understand the mechanisms of failure and assess the associated impacts. Among the 45 coseismic landslides identified, one landslide is situated within and six are adjacent to regions designated high-risk TSs (20 red dots in Fig. 2a) along the right-bank dip slope of the Zenwen Reservoir. Additionally, 21 coseismic landslides are concentrated along the right-bank dip slope of the Nanhua Reservoir; however, only two high-risk TSs are present in this area. Notably, the area of dip slope at Nanhua Reservoir is smaller than that at Zenwen Reservoir; otherwise, these landslides can likely be classified as high-risk TSs. Additionally, only ten landslides are situated on non-dip slopes, whereas the remainder of the landslides are found on dip slopes (as shown in Fig. 2a and detailed in Table 1).

4 Possible coseismic landslide early warning (CoLEW)

Timely early warning transmitted to nearby epicenter areas and public highway transportation networks are urgently needed for coseismic landslide hazard mitigation. According to detailed mapping of landslides using satellite images, approximately 45 landslides induced by this earthquake were concentrated in areas with PGA values > 250 gal (1 gal = 1 cm/s^2) (red line shown in Fig. 1a), which indicates all landslides triggered by the Dapu earthquake occurred within the PGA = 250 gal contour lines of earthquake shaking. The PGA is a critical factor triggering landslides, but it cannot provide timely warning for landslide sites. One possible way to issue a warning for coseismic landslides is to use the Pd amplitude. In this study, a Pd threshold of 0.3 cm was adopted to determine the LT, as shown in Fig. 1d, and the Pd = 0.3 cm contour line allows clear discrimination of potential landslide zones (blue line with Pd3 = 0.3 cm shown in Fig. 1a). For sites of coseismic landslides, the early warning LTs are 3–5 s ahead of the arrival of the PGA. Roadside landslides, which affects road sections, near strong-motion station CHY022, have an LT of approximately 4.48 s, which is sufficient for decision-making regarding emergency evacuation (Fig. 1d).

5 Conclusions

A total of 45 coseismic landslides, which were delineated by satellite images, with an average slope of 36.6° and an aspect of 136°, were triggered by the Dapu earthquake. Among these landslides, 35 were located on dip slopes, which implies that the bedding plane of the inclined rock layer was the critical geological factor for a case of the Dapu earthquake. In southern Taiwan, potential planar-failure dip slopes with slope areas less than 10 hectares should be also added as target slopes (TSs) in existing systems (CSS, https://css.lab.nycu.edu.tw; Lai et al. 2024) for coseismic landslide susceptibility mapping.

According to our results, Pd = 0.3 cm can be used as a CoLEW parameter to provide LTs ranging from 3 to 5 s (cyan area in Fig. 1b). In practice, selecting the Pd threshold depends on the purpose of early warning and requires different levels of tolerance for false or missed alarms. For inevitable and fatal coseismic landslides, having no missed alarm is critical to CoLEW applications where the cost of a missed alarm is high. In this study, a lower Pd threshold of 0.3 cm, which can capture 93.3% of earthquake-induced landslides, should be used to prevent missed alarm. In contrast, only 31% of coseismic landslides are encompassed by the 0.5 cm Pd contour line. We suggest that the Pd-based threshold method will be particularly useful for CoLEW target areas of crucial and fragile road sections. In addition, a low-cost earthquake early warning system (*P*-Alert) operated in Taiwan can provide additional real-time strong-motion data for proving the efficiency of on-site Pd estimation (Hsieh et al. 2014; Wu et al. 2025). However, the practical implementation of the proposed Pd-based onsite warning still has to be validated via more earthquakes. The Pd threshold value may change for different earthquake events because of the complexities in seismic response caused by subsurface geology and topographic effects, landslide

Table 1 Characteristics of the 45 coseismic landslides triggered by the Dapu earthquake

No	Longitude (°E)	Latitude (°N)	Collapsed area (m^2)	Mean slope (°)	Mean aspect (°)	Max elevation (m)	Strata[1]	Dip slope
1	120.553	23.294	1,841	30.61	108.10	589.09	Mp	YES
2	120.576	23.343	6,320	23.78	179.31	603.11	Al	YES
3	120.570	23.146	2,634	38.94	126.49	337.13	Ct	YES
4	120.601	23.224	15,290	39.40	203.14	659.87	Mp	YES
5	120.538	23.115	937	38.46	139.55	358.78	Al	YES
6	120.544	23.103	22,710	33.27	127.10	406.08	Ct	YES
7	120.545	23.103	47,492	30.62	128.78	337.57	Ct	YES
8	120.552	23.120	4,926	42.00	174.30	608.16	Mp	YES
9	120.470	23.078	5,681	14.31	156.83	110.72	Yc	NO
10	120.571	23.167	6,028	40.77	125.66	770.33	Al	YES
11	120.561	23.168	506	40.58	89.03	914.98	Tn	YES
12	120.562	23.170	1,936	55.22	112.58	1008.29	Tn	YES
13	120.567	23.171	3,389	45.89	137.37	794.11	Tn	YES
14	120.573	23.170	1,139	40.62	86.32	791.52	Al	YES
15	120.573	23.172	2,465	48.09	99.76	854.36	Al	YES
16	120.464	23.179	2,007	44.22	172.39	239.69	Ct	YES
17	120.579	23.180	2,514	47.73	155.62	607.52	Al	YES
18	120.576	23.180	4,060	49.21	135.41	762.47	Al	YES
19	120.576	23.194	2,682	25.71	56.38	1007.78	Ys	NO
20	120.547	23.275	7,379	44.83	208.62	458.73	Al	YES
21	120.584	23.186	1,922	46.63	191.27	569.19	Al	YES
22	120.608	23.085	3,880	16.73	250.50	333.58	Al	NO
23	120.602	23.381	27,083	27.97	143.81	1014.75	Cc	YES
24	120.540	23.157	729	42.37	203.37	530.37	Ct	NO
25	120.569	23.157	1,174	34.53	139.56	458.79	Al	YES
26	120.569	23.157	1,044	36.80	149.97	441.18	Al	YES
27	120.553	23.135	6,591	36.20	120.90	553.03	Al	YES
28	120.499	23.122	1,138	34.03	84.03	159.93	Pa	NO
29	120.502	23.126	1,498	15.50	162.42	111.55	Pa	NO
30	120.511	23.121	1,903	36.67	141.79	173.78	Ct	NO
31	120.525	23.146	789	41.17	206.65	351.20	Ct	NO
32	120.531	23.151	1,248	37.48	99.50	392.88	Ct	NO
33	120.533	23.144	21,020	30.68	213.67	418.25	Ct	NO
34	120.584	23.186	2,267	39.98	116.47	573.16	Al	YES
35	120.599	23.365	4,797	34.07	101.12	1120.50	Tn	YES
36	120.600	23.366	6,091	28.62	95.06	1053.10	Tn	YES
37	120.613	23.367	8,311	21.59	111.44	514.58	Ys	YES
38	120.611	23.367	5,726	19.65	121.04	587.63	Tn	YES
39	120.562	23.152	3,718	44.49	110.98	769.98	Al	YES
40	120.562	23.152	2,962	46.67	143.44	736.46	Al	YES
41	120.563	23.153	2,059	44.42	110.70	707.51	Al	YES
42	120.494	23.227	1,633	40.82	85.82	296.12	Tn	YES
43	120.493	23.228	1,909	37.36	81.01	332.08	Tn	YES
44	120.493	23.229	4,035	38.59	100.63	422.04	Tn	YES
45	120.653	23.175	2,651	39.21	111.33	560.58	Tn	YES

[1] Formations (from old to young): Late Miocene for **Cc** (Changchihkeng Formation), **Tn** (Tangenshan Sandstone); Early Pliocene for **Ys** (Yenshuikeng Shale), **Al** (Ailiaochiao Formation), **Mp** (Maopu Shale); Late Pliocene: **Ct** (Chutouchi Formation); Pleistocene for **Pa** (Peiliao shale), **Yc** (Yuching Shale)

source types (e.g., rockfalls, shallow slides, deep-seated landslides) and the strength of landslide materials.

Acknowledgements
The authors acknowledge the Central Weather Administration, Taiwan, for the TSMIP seismic waveforms (https://gdms.cwa.gov.tw/, last accessed February 2025). This study is financially supported by the National Science and Technology Council of Taiwan (NSTC) for Wei-An Chao under grants NSTC 111-2628-M-A49-003 and NSTC 113-2124-M-239-001 and for Che-Ming Yang under grants NSTC 113-2116-M-239-001 and was partly supported by the Agency of Rural Development and Soil and Water Conservation (ARDSWC) for Wei-An Chao under Grants ARDSWC-112-050 and ARDSWC-113-094. The authors also acknowledge BigGIS (https://gis.ardswc.gov.tw/), ARDSWC, Taiwan, for providing satellite images of Sentinel-2 data from December 20, 2024, and January 24, 2025; the Chiayi Branch, Forestry and Nature Conservation Agency, Taiwan, for providing field photographs; and the Geological Survey and Mining Management Agency, Taiwan, for providing LiDAR slope maps. The imagery data for landslide mapping are sublicensed by AIRBUS DS from the Center for Space and Remote Sensing Research (CSRSR), National Central University (NCU). For SPOT 6 imagery data: "© Airbus DS (2024)". The satellite image date of SPOT6 is January 22, 2025.

Author contributions
W.A. performed the seismic data processing, and was responsible for the overall design and operation of this research. W.A., C.M. and K.S. wrote the manuscript. K.S. and T.S. assisted in implementing the coseismic landslide susceptibility mapping and editing of the manuscript. C.M. assisted in creating the coseismic landslide inventory, and was involved in the interpretation of the results. Y.M. contributed to the editing and interpretation.

Data availability
No datasets were generated or analysed during the current study.

Declarations

Competing interests
The authors declare no competing interests.

Received: 20 February 2025 Accepted: 1 April 2025
Published online: 11 April 2025

References

Chang JM, Chao WA, Yang CM, Huang MW (2024) Coseismic and subsequent landslides of the 2024 Hualien earthquake (M7.2) on April 3 in Taiwan. Landslides. https://doi.org/10.1007/s10346-024-02312-x

Chousianitis K, Del Gaudio V, Sabatakakis N, Kavoura K, Drakatos G, Bathrellos GD, Skilodimou HD (2016) Assessment of earthquake-induced landslide hazard in Greece: from arias intensity to spatial distribution of slope resistance demand. Bull Seism Soc Am 106(1):174–188

Chuang RY, Wu BS, Liu HC, Huang HH, Lu CH (2021) Development of a statistics-based nowcasting model for earthquake-triggered landslides in Taiwan. Eng Geol. https://doi.org/10.1016/j.enggeo.2021.106177

Colombelli S, Amoroso O, Zollo A, Kanamori H (2012) Test of a threshold-based earthquake early warning method using Japanese data. Bull Seismol Soc Am 102(3):1266–1275. https://doi.org/10.1785/0120110149

Fei LY, Chen MM (2013) Geological investigation and database construction for upstream of flood-prone area – Maps and Explanatory text. Central Geological Survey, MOEA, Taiwan. 192pp.

Guzzetti F, Carrara A, Cardinali M, Reichenbach P (1999) Landslide hazard evaluation: a review of current techniques and their application in a multi-scale study, Central Italy. Geomorphology 31:181–216. https://doi.org/10.1016/s0169-555x(99)00078-1

Harp EL, Wilson RC (1995) Shacking intensity thresholds for rock falls and slides: evidence from 1987 Whittier narrows and superstition hills earthquake strong-motion records. Bull Seism Soc Am 85(6):1739–1757

Harp EL, Hartzell SH, Jibson RW, Ramirez-Guzman L, Schmitt RG (2014) Relation of landslides triggered by the Kiholo Bay earthquake to modeled ground motion. Bull Seism Soc Am 104(5):2529–2540. https://doi.org/10.1785/0120140047

Hsieh CY, Wu YM, Chin TL, Kuo KH, Chen DY, Wang KS, Chan YT, Chang WY, Li WS, Ker SH (2014) Low cost seismic network practical applications for producing quick shaking maps in Taiwan. Terr Atmos Ocean Sci 25:617–624. https://doi.org/10.3319/TAO.2014.03.27.01(T)

Hsieh CY, Chao WA, Wu YM (2015) Earthquake early warning approach using a low-cost seismic network. Seismol Res Lett. https://doi.org/10.1785/0220150073

Keefer DK (1994) The importance of earthquake-induced landslides to long-term slope erosion and slope-failure hazards in seismically active regions. Geomorphology 10:265–284

Lai TS, Chao WA, Yang CM, Wu YM, Chang JM, Chen DY, Wu CF (2024) Rapid coseismic landslide susceptibility assessment via Newmark analysis, the decision tree algorithm, and a web-based display system. Eng Geol. https://doi.org/10.2139/ssrn.5095533

Lee CT (2014) Statistical seismic landslide hazard analysis: an example from Taiwan. Eng Geol 182:201–212. https://doi.org/10.1016/j.enggeo.2014.07.023

Lin CW, Lu ST, Shih TS, Liu YC, Lin WH, Lin YH (2007) Active faults of southwestern Taiwan—explanatory text for the strip maps of active faults. Central Geol Sur Sp Publ 17:141

Lin CW, Chen WS, Liu YC, Chen PT (2009) Chaochou fault. Special Publ Central Geol Sur 23:133–148

Lin CW, Liu YC, Chou PS, Lin YH (2021) Recent development of active fault investigations of Taiwan. Bull Central Geol Sur 34:1–40

Nowicki Jessee MA, Hamburger MW, Allstadt K, Wald DJ, Robeson SM, Tanyas H, Hearne M, Thompson EM (2018) A global empirical model for near real-time assessment of seismically induced landslides. J Geophys Res: Earth Surface 123(8):1835–1859. https://doi.org/10.1016/0169-555X(94)90021-3

Pham BT, Prakash I, Bui DT (2018) Spatial prediction of landslides using a hybrid machine learning approach based on random subspace and classification and regression trees. Geomorphology 303:256–270. https://doi.org/10.1016/j.geomorph.2017.12.008

Rault C, Chao WA, Gellis C, Burtin A, Chang JM, Marc O, Lai TS, Wu YM, Hovius N, Meunier P (2020) Seismic response of a mountain ridge prone to landsliding. Bull Seismol Soc Am 110:3004–3020. https://doi.org/10.1785/0120190127

Shieh JT, Wu YM, Zhao L, Chao WA, Wu CF (2011) An examination of τ_c-Pd earthquake early warning method using a strong-motion building array. Soil Dyn Earthq Eng 31:240–246

Wu YM, Kanamori H (2005) Rapid assessment of damage potential of earthquakes in Taiwan. Bull Seismol Soc Am 95(3):1181–1185. https://doi.org/10.1785/0120040193

Wu YM, Lin TL, Chao WA, Huang HH, Hsiao NC, Chang CH (2011) Faster short-distance earthquake early warning using continued monitoring of filtered vertical displacement: a case study for the 2010 Jiasian, Taiwan, Earthquake. Bull Seismol Soc Am 101(2):701–709. https://doi.org/10.1785/0120100153

Wu YM, Liang WT, Mittal H, Chao WA, Lin CH, Huang BS, Lin CM (2016) Performance of a low-cost earthquake early warning system (P-Alert) during the 2016 ML 6.4 Meinong (Taiwan) Earthquake. Seismol Res Lett. https://doi.org/10.1785/0220160058

Wu YM, Lin YH, Yang BM, Ke SS (2025) Performance of the P-Alert real-time shakemaps system and onsite warning during the 2025 ML 64 Dapu earthquake, accepted by Terrestrial. Atmospheric Ocean Sci. https://doi.org/10.1007/s44195-025-00086-w

Zhu W, Beroza GC (2019) PhaseNet: a deep-neural-network-based seismic arrival-time picking method. Geophys J Int 216:261–273. https://doi.org/10.1093/gji/ggy423

Publisher's Note

Springer Nature remains neutral with regard to jurisdictional claims in published maps and institutional affiliations.